

Loss of functional ELOVL4 depletes very long-chain fatty acids (\geq C28) and the unique ω -O-acylceramides in skin leading to neonatal death

Vidyullatha Vasireddy^{1,†}, Yoshikazu Uchida^{2,†}, Norman Salem Jr³, Soo Yeon Kim³, Md Nawajesh Ali Mandal¹, Geeredy Bhanuprakash Reddy⁴, Ravi Bodepudi¹, Nathan L. Alderson⁵, Johnie C. Brown⁶, Hiroko Hama⁵, Andrzej Dlugosz⁷, Peter M. Elias², Walter M. Holleran^{2,8} and Radha Ayyagari^{1,*}

¹Department of Ophthalmology and Visual Sciences, University of Michigan, Ann Arbor, MI 48105, USA,

²Department of Dermatology, School of Medicine, University of California, San Francisco, and Veterans Administration Medical Center, San Francisco, CA 94121, USA, ³Laboratory of Membrane Biochemistry and Biophysics, NIAAA, National Institutes of Health, Bethesda, MD 20892, USA, ⁴National Institute of Nutrition, Hyderabad, India, ⁵Department of Biochemistry and Molecular Biology, Medical University of South Carolina, Charleston, SC 29425, USA, ⁶Applied Biosystems, Framingham, MA 01701, USA, ⁷Department of Dermatology, University of Michigan, Ann Arbor, MI 48109, USA and ⁸Department of Pharmaceutical Chemistry, School of Pharmacy, University of California, San Francisco, CA 94143, USA

Received November 15, 2006; Revised December 22, 2006; Accepted December 28, 2006

Mutations in elongation of very long-chain fatty acid-4 (*ELOVL4*) are associated with autosomal dominant Stargardt-like macular degeneration (STGD3), with a five base-pair (5 bp) deletion mutation resulting in the loss of 51 carboxy-terminal amino acids and truncation of the protein. In addition to the retina, *Elovl4* is expressed in a limited number of mammalian tissues, including skin, with unknown function(s). We generated a knock-in mouse model with the 5-bp deletion in the *Elovl4* gene. As anticipated, mice carrying this mutation in the heterozygous state (*Elovl4*^{+/*del*}) exhibit progressive photoreceptor degeneration. Unexpectedly, homozygous mice (*Elovl4*^{*del/del*}) display scaly, wrinkled skin, have severely compromised epidermal permeability barrier function, and die within a few hours after birth. Histopathological evaluation of the *Elovl4*^{*del/del*} pups revealed no apparent abnormality(ies) in vital internal organs. However, skin histology showed an abnormally-compacted outer epidermis [stratum corneum (SC)], while electron microscopy revealed deficient epidermal lamellar body contents, and lack of normal SC lamellar membranes that are essential for permeability barrier function. Lipid analyses of epidermis from *Elovl4*^{*del/del*} mice revealed a global decrease in very long-chain fatty acids (VLFAs) (i.e., carbon chain \geq C28) in both the ceramide/glucosylceramide and the free fatty-acid fractions. Strikingly, *Elovl4*^{*del/del*} skin was devoid of the epidermal-unique ω -O-acylceramides, that are key hydrophobic components of the extracellular lamellar membranes in mammalian SC. These findings demonstrate that ELOVL4 is required for generating VLFA critical for epidermal barrier function, and that the lack of epidermal ω -O-acylceramides is incompatible with survival in a desiccating environment.

*To whom correspondence should be addressed at: Department of Ophthalmology and Visual Sciences, W.K. Kellogg Eye Center, 1000 Wall Street, Ann Arbor, MI 48105, USA. Tel: +1 7346476345; Fax: +1 7349367231; Email: ayyagari@umich.edu

[†]These authors contributed equally to this work.

Published by Oxford University Press 2007.

The online version of this article has been published under an open access model. Users are entitled to use, reproduce, disseminate, or display the open access version of this article for non-commercial purposes provided that: the original authorship is properly and fully attributed; the Journal and Oxford University Press are attributed as the original place of publication with the correct citation details given; if an article is subsequently reproduced or disseminated not in its entirety but only in part or as a derivative work this must be clearly indicated. For commercial re-use, please contact: journals.permissions@oxfordjournals.org

INTRODUCTION

Mutations in the elongation of very long-chain fatty acid-4 (*ELOVL4*) gene are implicated in autosomal dominant Stargardt-like macular degeneration (STGD3) (1,2). The structure of *ELOVL4* protein is homologous to mammalian and yeast ELO family of proteins that are involved in the 'carbon' chain elongation of long-chain fatty acids (2). In addition to retina, *Elov4* expression has been detected in brain, whole skin and testis in mouse (3), suggesting role(s) for *ELOVL4* in these tissues. On the basis of structural homology of *ELOVL4* with the ELO family of proteins and the importance of docosahexaenoic acid (C22:6 n-3) for the function of photoreceptors in the eye, it has been proposed that the *ELOVL4* protein may play a key role in fatty acid (FA) metabolism (2). However, direct evidence for *ELOVL4* involvement in FA metabolism has not yet been established.

Three mutations associated with macular degeneration have been reported in the *ELOVL4* gene to date. All three mutations are located in the last exon (exon 6), resulting in the truncation of the protein and loss of the C-terminal ER retention signal (2,4,5). In a heterologous system, a 5-bp deletion mutant *ELOVL4* demonstrated a dominant-negative effect by interacting and recruiting wild-type (Wt) protein into aggresomes (6). To assess the consequences of the 5-bp deletion mutation *in vivo*, we developed a knock-in mouse model carrying the *Elov4* 5-bp deletion. Mice carrying the mutation in the heterozygous state (*Elov4*^{+del}) were viable and developed progressive photoreceptor degeneration (7), whereas homozygous neonates (*Elov4*^{del/del}) died within a few hours after birth.

During epidermal differentiation, keratinocytes proliferate in the inner-most cell layer (basal), and then migrate toward the outer surface of the skin (8). The outermost layers of the epidermis are responsible for critical protective functions, including, most-importantly, permeability barrier homeostasis; i.e., prevention of excess transcutaneous water loss, a function required for survival of mammals in a desiccating, terrestrial environment. The epidermal permeability barrier to water loss resides in the extracellular domains of the stratum corneum (SC), where a hydrophobic lipid mixture is organized into distinctive multi-lamellar membranous structures, comprised primarily of free fatty acids (FFAs), cholesterol and ceramides (9). Precursors for these barrier lipids are stored in the epidermal lamellar bodies (LB), generated within the outer nucleated layers of the epidermis (10). The quantity of LB in the cytosol increases during epidermal differentiation, followed by their fusion with the apical plasma membrane of the outer-most nucleated cell layer of the epidermis. Secretion of LB contents into the inter (extra)-cellular spaces between the stratum granulosum (SG) and SC is followed by enzymatic processing of lipid precursors, eventually forming the extracellular lamellar bilayers that mediate permeability barrier function(s) (11).

Three families of lipids, cholesterol, FFA and ceramides present in an approximate 1:1:1 molar ratio, form the extracellular lamellar membranes that mediate epidermal permeability barrier homeostasis (12). A lipid monolayer composed primarily of ω -hydroxyceramides, but also including omega-hydroxy and non-hydroxy FFAs and other minor ceramide species (13,14) covalently linked to peptides on

the outer portion of highly-crosslinked cornified envelope (CE) proteins, links this hydrophobic extracellular matrix to the corneocytes, forming a two-compartment structure in the SC, which has been analogized to a 'brick and mortar' model (15–18). Inhibited or acquired abnormalities, leading to structural defects in either the lipid-enriched 'mortar' or the proteinaceous 'bricks' occur in several cutaneous syndromes, resulting in abnormal barrier function with attendant hyperkeratosis ('ichthyoses') (19), highlighting the importance of both of these compartments for epidermal function.

Here, we report that loss of functional *ELOVL4* results in abnormal epidermal permeability barrier structure and function, and given that no abnormalities were noted in other major organ tissues, including brain, liver, kidney and lung, the loss of skin barrier function appears to be the primary cause of the early neonatal demise of these animals. Thus, *ELOVL4* normally has a critical, previously-unreported role in epidermal permeability barrier function and mammalian survival in the post-natal, desiccating, terrestrial environment. We demonstrate further that *ELOVL4* is essential for the synthesis of epidermal very long-chain FA (VLFA), and is required for generating ω -O-acylceramides, a key ceramide molecular species that is essential for permeability barrier function. Loss of *ELOVL4*-generated VLFA and ω -O-acylceramides are likely to be the underlying cause of the early demise in mice with the homozygous 5 bp-deletion mutant.

RESULTS

Tissue-specific distribution of different *Elovl*s

Distribution of the expression for different *Elovl* genes (*Elovl1*–*Elovl6*) in control C57BL/6 animals was analyzed by qRT-PCR (Fig. 1). *Elovl1* mRNA expression was evident in mouse liver, skin, retina and brain, with highest expression in liver. In contrast, a high level of *Elovl2* expression was also detected in liver, but very low expression was observed in retina, with no detectable expression in either skin or brain. High levels of *Elovl3* were evident in liver, with low expression detected in skin; no *Elovl3* expression was detected in either retina or brain. Consistent with earlier observations (3), *Elovl4* was detected in murine skin, retina and brain, with no expression detected in liver. Expression of *Elovl5* and *Elovl6* was highest in liver, whereas brain and retina showed low levels of expression. Expression of *Elovl5* and *Elovl6* was not detected in skin, while all other *Elovl* genes, with the exception of *Elovl4*, being expressed in liver (Fig. 1). This differential expression of *Elovl* genes likely reflects tissue-specific requirement for different FA in normal murine tissues.

Expression of *Elov4* 5-bp deletion mutation in skin of knock-in mice

Semi-quantitative RT-PCR analysis of cDNA from whole skin (including both dermis and epidermis) of newborn *Elov4* 5-bp deletion mutant knock-in mice using primers designed to specifically amplify either the Wt or mutant *Elov4* alleles confirmed the expression of both Wt and

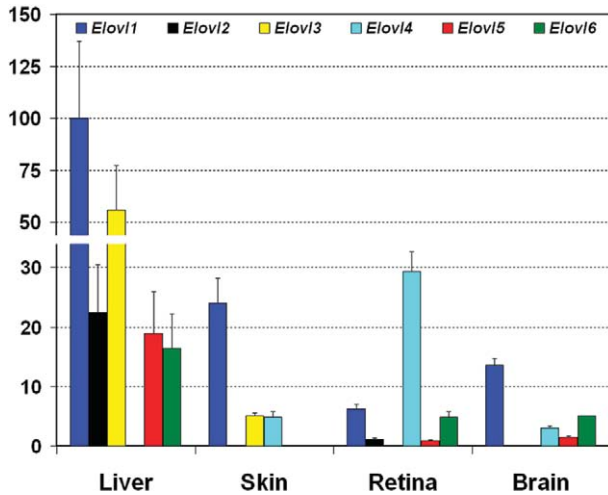


Figure 1. Tissue-specific distribution of *Elov1*–*Elov6*. Expression of *Elov1*–*Elov6* in mouse liver, skin, retina and brain was determined by qRT–PCR. Data are presented on an arbitrary scale after normalization with the housekeeping-gene glyceraldehyde 3-phosphate dehydrogenase (*Gapdh*). The values are the means [\pm standard deviation (SD)] for at least three independent observations.

mutant *Elov4* transcripts in the skin of heterozygous (*Elov4*^{+/*del*}) mice, whereas only the mutant transcript was detected in the skin of homozygous knock-in *Elov4*^{*del/del*} animals (Fig. 2A). The expression level of the mutant transcript in *Elov4*^{*del/del*} skin was approximately double that in *Elov4*^{+/*del*} littermates. As expected, Wt littermates expressed only the Wt allele.

Immunoblot analysis of ELOVL4 protein in the skin of *Elov4*^{*del/del*} animals, detected only the mutant protein (33 kDa) (Fig. 2B), whereas the skin of *Elov4*^{+/*del*} animals contained both the Wt (37 kDa) and mutant proteins (Fig. 2B); again Wt control mice expressed only Wt protein. These results are consistent with the observations presented earlier, and confirm that a truncated ELOVL4 protein is produced in the skin of mice carrying the mutant allele(s).

Early postnatal lethality, abnormal skin phenotype and defective barrier function in *Elov4*^{*del/del*} mice

The offspring of *Elov4*^{+/*del*} matings were closely monitored from birth. Although *Elov4*^{*del/del*} mice were indistinguishable from littermate Wt controls immediately after birth, careful monitoring and subsequent genotyping revealed high postnatal lethality of *Elov4*^{*del/del*} animals. No significant differences in birth weight were evident for animals with each of the three genotypes. However, the *Elov4*^{*del/del*} animals were not fed by their mothers, and died within 4 h after birth. By 3 h after birth, the *Elov4*^{*del/del*} animals appeared smaller in size and developed an abnormal gross appearance (Fig. 3A); i.e., their skin appeared more fragile, darker in color, scaly and drier (Fig. 3A), when compared with either heterozygous or Wt littermates.

The dry, scaly skin and progressive loss of body weight in *Elov4*^{*del/del*} mice suggested a possible defect in fluid retention due to altered skin barrier function. To evaluate evaporative

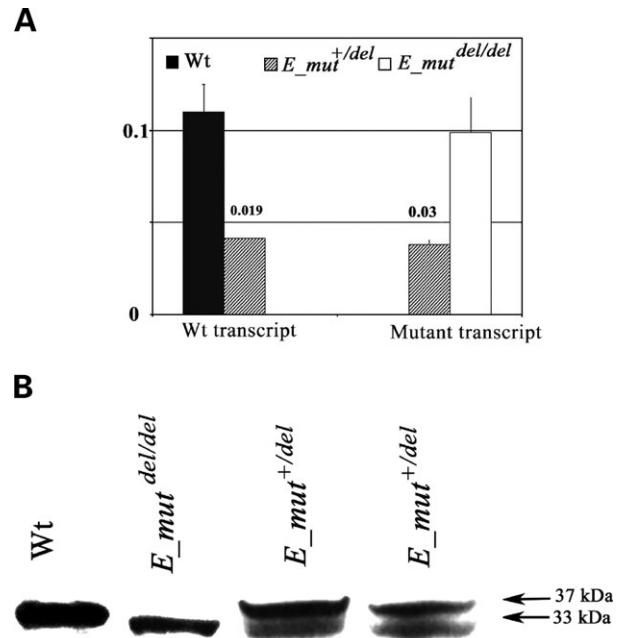


Figure 2. Expression profile of *Elov4* transcripts (A) and protein (B) in *Elov4*^{*del/del*}, *Elov4*^{+/*del*} and Wt mice. The expression profile of Wt and mutant transcripts (A) and proteins (B) in skin was evaluated and compared with *Elov4*^{*del/del*}, *Elov4*^{+/*del*} and Wt animals. *Elov4*^{*del/del*} mice expressed only mutant transcript (A), whereas *Elov4*^{+/*del*} animals expressed both the Wt and mutant transcript to near identical levels (A). As expected, Wt mice did not express the mutant allele in their skin. Data are presented as the fold-change relative to the expression of the housekeeping-gene, hypoxanthine guanine phosphoribosyl transferase (*Hgprt*). The expression values represent the mean (\pm SD) for at least three independent observations. (B) Immunoblot analysis of skin homogenates showed the expression of mutant protein alone in *Elov4*^{*del/del*} (33 kDa), both Wt (37 kDa) and mutant (33 kDa) proteins in *Elov4*^{+/*del*} mice, and only Wt protein in Wt animals (B). Immunoblot analysis was performed using anti-ELOVL4 antibodies.

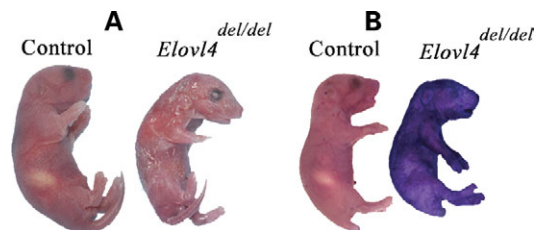


Figure 3. Phenotype of *Elov4*^{*del/del*} in newborn mice. *Elov4*^{*del/del*} mice show epidermal abnormalities, and defective epidermal permeability barrier (A and B). Comparison of *Elov4*^{*del/del*} and Wt-littermate pups at postnatal day 0 revealed abnormal appearance of skin in *Elov4*^{*del/del*} pups. *Elov4*^{*del/del*} pups show a scaly, red and shiny skin (A). Penetration assay with haematoxylin revealed a defective epidermal permeability barrier function in *Elov4*^{*del/del*} skin (B). Animals from three different litters were used to perform the dye-exclusion assay, with representative results shown.

fluid loss in *Elov4*^{*del/del*} mice, we next compared the total body weights of animals 3 h after birth. The body weights of *Elov4*^{*del/del*} mice were significantly lower than either *Elov4*^{+/*del*} or Wt animals ($P < 0.001$) (data not shown). The scaly, red skin and the decrease in body weight of the *Elov4*^{*del/del*} mice are consistent with compromised epidermal barrier function in these animals.

A standard, dye exclusion assay for permeability barrier function using haematoxylin whole mount staining (20) revealed dark staining of homozygous (*Elovl4^{del/del}*) neonates, indicating extensive dye penetration and defective skin barrier function (Fig. 3B). In contrast, dye penetration was not evident in Wt newborn animals (Fig. 3B), consistent with the expected normal barrier function shortly after birth. These results demonstrate defective epidermal permeability barrier function exclusively in homozygous *Elovl4^{del/del}* mouse skin.

Histopathological and ultrastructural evaluation of epidermis in *Elovl4^{del/del}* mice

To further assess the basis for the early postnatal lethality in *Elovl4^{del/del}* mice, we examined the histology of skin and other key organs. Histopathological evaluation of vital organs including lungs, heart, brain and kidney revealed no significant abnormality(ies) in *Elovl4^{del/del}* animals (data not shown), with the exception of epidermis. Detailed histopathological analysis of skin samples from *Elovl4^{del/del}* animals from different body sites, including eyelids, hindlimb, foot pads and the dorsal side of the body trunk from at least three different *Elovl4^{del/del}* animals showed relatively normal-appearing morphology of the nucleated (viable) epidermal cell layers compared with littermate *Elovl4^{+/-del}* and Wt control animal epidermis. However, the SC, the outermost layers of the epidermis, appeared disorganized and more compact in *Elovl4^{del/del}* mice than in *Elovl4^{+/-del}* and Wt littermates (Fig. 4A).

To gain further insights into the structural basis of the barrier abnormality in *Elovl4^{del/del}* mice, we next assessed epidermal ultrastructure both by standard electron microscopy and with a lipid-retaining fixative, ruthenium tetroxide (21). While the density (i.e., number) of LB in the cytosol of granular (SG) cells did not differ in *Elovl4^{del/del}* when compared with *Elovl4^{+/-del}* or Wt animals (data not shown), there were marked abnormalities in the contents of these organelles (Fig. 4B). Specifically, vesicles containing electron-dense, amorphous material were co-assembled with normal-appearing lamellar material within nascent LB in the *trans*-Golgi (Fig. 4Biii). These vesicles often appeared to fuse with similar microvesicles within the same organelles, or immediately after secretion at the SG–SC interface (Fig. 4Biv), forming large, non-lamellar spheres within the extracellular spaces (Fig. 4Biv, asterisks). In contrast, the secreted contents of LB in Wt epidermis formed a uniform lamellar phase; with the normal reorganization into broad lamellar membranes within the SG–SC interface evident (Fig. 4Bi, arrows). While secreted lamellar material formed lamellar membranes that filled the extracellular spaces in Wt SC, the lamellar material in *Elovl4^{del/del}* epidermis failed to transform into a uniform lamellar membrane phase within the SC interstices (Fig. 4Bii). These results demonstrate that the defective permeability barrier in *Elovl4^{del/del}* can be attributed to abnormalities in LB contents and the subsequent failure of these abnormal contents to organize into the replete extracellular lamellar bilayers required for normal cutaneous barrier function.

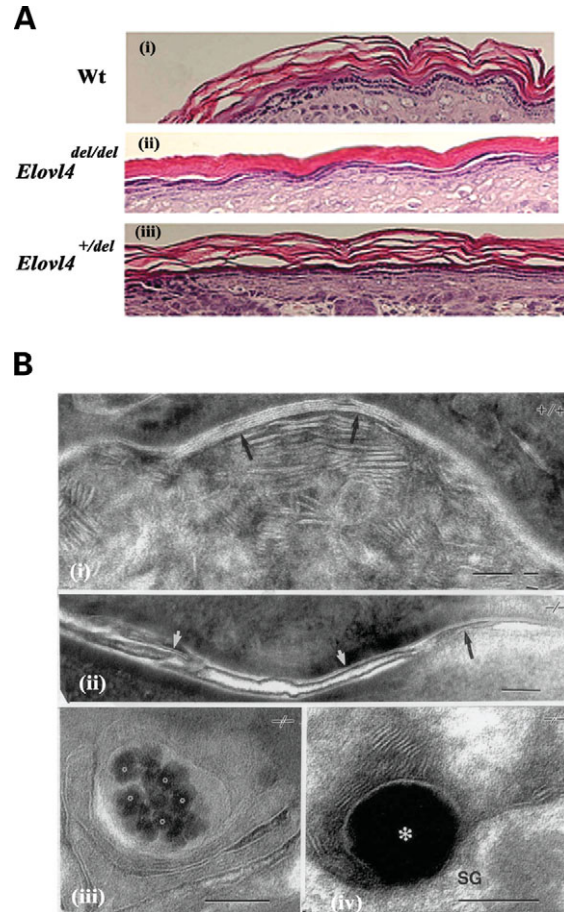


Figure 4. Comparison of control and *Elovl4^{del/del}* mutant epidermis by histology and transmission electron microscopy. H&E-stained paraffin sections (Ai–iii), thin sections (Bi–iv), revealed significant differences in SC morphology (A) and alterations in LB contents and lamellar membrane organization in *Elovl4^{del/del}* epidermis (B). Epidermis from Wt mice shows a normal pattern of secreted, lamellar contents at the SG–SC interface (Bi), which reorganizes into broad lamellar membrane sheets (arrows). Bii–Biv show electron-dense, spherical inclusions present within nascent LB at the level of the *trans*-golgi in *Elovl4^{del/del}* mice (Biii, asterisks). These abnormal lipid contents tend to coalesce into larger droplets, which are co-secreted with lamellar contents at the SG–SC interface (Biv, asterisk). Secreted lamellar and abnormal, non-lamellar contents fail to reorganize into replete, lamellar membrane bilayers within extracellular domains of *Elovl4^{del/del}* SC (Bii). Bii–Biv, ruthenium tetroxide post-fixation; Mag bars = 0.1 μ m. Representative animals from three different litters were used to evaluate the histology.

Analysis of epidermal differentiation markers

Epidermal differentiation comprises an orchestrated, vertical transformation of keratinocytes into the enucleate SC layer, forming the epidermal permeability barrier function. Mutations of a number of proteins expressed in the differentiated layers of epidermis occur in hereditary cutaneous disorders, and are accompanied by compromised epidermal barrier function, e.g., mutations of lorricrin, involucrin and transglutaminase (22). Because ELOVL4 has been suggested to be involved in the synthesis of unsaturated VLFA and their metabolites, eicosanoids, which can regulate epidermal proliferation and differentiation (23), we next examined the expression patterns of specific protein markers in *Elovl4^{del/del}*

and Wt control neonatal epidermis by immunofluorescence. Consistent differences in epidermal marker expression were not observed between control and *Elovl4^{del/del}* mice (data not shown). The expression pattern of these markers suggests not only normal epidermal differentiation in the homozygous, knock-in mice, but also that the permeability barrier defect in *Elovl4^{del/del}* mice is likely due instead to alterations in the lipid-enriched, extracellular matrix.

Lipid composition of *Elovl4^{del/del}* and Wt mouse epidermis

Since it is well established that cholesterol, FFA and ceramide are the three major lipid classes critical for permeability barrier formation and function, we next measured the content of these lipids in the knock-in and Wt epidermis. Interestingly, the total content of these three lipid classes was not significantly altered in the *Elovl4^{del/del}* versus Wt epidermis (Table 1). In addition, the content of glucosylceramide and sphingomyelin, both of which are precursors in the formation of the SC ceramides critical for mammalian epidermal permeability barrier (11,24) also were unaltered in epidermis from *Elovl4^{del/del}* (Table 1). However, because mammalian epidermis contains at least nine major ceramide molecular species with distinct combinations of sphingol base structures and amide-linked FA (25,26), we further analyzed the FA composition of the amide-linked FA of epidermal ceramide/glucosylceramide by GLC-MS. The *N*-acyl-VLFA of the combined epidermal ceramide/glucosylceramide fraction [i.e., non-hydroxy (non-OH) FA (>C30); α -OH FA (\geq C28); ω -OH FA (>C30)] was significantly diminished or not detectable (n.d.) in *Elovl4^{del/del}* epidermis (Table 2). In contrast, shorter chain length *N*-acyl FA of ceramide/glucosylceramide (i.e. non-OH C18 and C26; α -OH, C16 & C26; ω -OH C18 and C20) were elevated in *Elovl4^{del/del}* epidermis (Table 2). Consistent with changes in amide-linked FA of ceramide/glucosylceramides, the composition of free VLFA was also altered [i.e., non-OH FFA (>C28), 2-OH FFA (>C26) and ω -OH FFA (>C28)], were either not detectable or markedly diminished in *Elovl4^{del/del}* compared with Wt epidermis (Table 3). These results suggest that lack of competent epidermal permeability barrier structure/formation is attributable either to a deficiency of VLFA and/or an alteration of the FA composition within the ceramide/glucosylceramide fractions, rather than a global decrease in lipid content within the epidermis.

Mammalian epidermis contains unique ω -O-acylceramide species that contain VLC *N*-acyl FA and are critical for the formation of lamellar membrane structures (27). Given that diminished content of these epidermal-unique ω -O-acylceramides is associated with a variety of cutaneous disorders, including atopic dermatitis, lamellar ichthyosis and Sjogren-Larssen syndrome with barrier abnormalities (28), we specifically examined the ω -O-acylceramide content and FA composition in the epidermis. High performance-TLC analysis of total lipid extracts from *Elovl4^{del/del}* epidermis revealed undetectable levels of both ω -O-acylceramide and its immediate precursor, acylglucosylceramide (acylGlcCer) (Fig. 5). In contrast, all other ceramide and glucosylceramide species were present in near-normal amounts in *Elovl4^{del/del}* compared with Wt control epidermis (Fig. 5). High performance liquid chromatography-atmospheric pressure chemical ionization

Table 1. Epidermal lipid content

	Wt (μ g/mg dry tissue)	<i>del/del</i> (μ g/mg dry tissue)
Cholesterol	13.5 \pm 4.12	17.2 \pm 0.95
FFA	11.5 \pm 3.39	11.0 \pm 0.18
Ceramide	11.9 \pm 1.10	13.0 \pm 0.84
Glucosylceramide	1.95 \pm 0.22	2.15 \pm 0.37
Sphingomyelin	2.82 \pm 0.26	3.11 \pm 1.15

Values represent mean \pm SD from four mice.

Table 2. Profiles of amide-linked FA of epidermal ceramide/glucosylceramide

	Non-OH FA ^a		α -OH FA ^a		ω -OH FA ^a	
	Wt	<i>del/del</i>	Wt	<i>del/del</i>	Wt	<i>del/del</i>
12:0	0.53	0.75	0.37	1.44	1.95	2.40
14:0	1.42	1.77	0.33	2.87	n.d.	n.d.
16:0	13.9	18.9	27.6	83.6	1.10	0.42
18:0	9.6	18.8	0.48	1.99	7.80	13.3
18:1	n.d.	n.d.	0.03	n.d.	2.89	3.55
20:0	0.22	0.40	1.79	2.4	33.9	41.4
22:0	6.84	4.18	2.59	n.d.	26.2	19.9
24:0	6.14	10.3	10.9	n.d.	7.05	4.17
24:1	n.d.	n.d.	29.4	n.d.	11.2	8.41
26:0	16.9	42.3	1.28	7.73	4.05	5.68
28:0	1.28	1.57	25.2	n.d.	n.d.	n.d.
30:0	43.0	0.98	n.d.	n.d.	1.75	0.75
32:0	0.12	n.d.	n.d.	n.d.	2.14	n.d.
34:0	0.09	n.d.	n.d.	n.d.	n.d.	n.d.
Total	100	100	100	100	100	100
Total ^b						
	Wt	<i>del/del</i>				
Total Non-OH	203.3	188.9				
Total α -OH	62.9	19.9				
Total ω -OH	30.8	45.3				
Total	297.0	254.1				

n.d., not detectable.

Carbon chain lengths for saturated FA (C12–C34) and unsaturated FA (C18:1 and C24:1), which are present in epidermal ceramides and glucosylceramides, were assessed; polyunsaturated fatty acids were not quantified in epidermis (47).

^aData are reported as mol % of total FFA.

^bData are reported as nmol/mg of dry epidermis.

tandem mass spectrometry (HPLC-APCI-MS/MS) studies confirmed the presence of ω -O-acylceramides and their identified molecular species in Wt epidermis (Fig. 6A, upper panel and 6B), but these unique ω -O-acylceramides were not detected in *Elovl4^{del/del}* epidermis (Fig. 6A, lower panel). These results strongly suggest that ELOVL4 accounts for generation of ceramides and glucosylceramides containing VLFA, and that a lack of normal ELOVL4 function not only alters the VLFA composition, but also eliminates the production of a key epidermal barrier ceramide species, ω -O-acylceramide and its immediate precursors, ω -O-acylglucosylceramide.

On the basis of sequence homology between ELOVL4 and yeast FA elongases, the ELOVL4 is predicted to have a role in the generation of polyunsaturated FA (PUFA) (2). Given that the isolation of epidermis from whole skin likely alters the levels of labile PUFA, we determined the FA composition in

Table 3. Profiles of epidermal FFA

	Non-OH ^a		α-OH ^a		ω-OH	
	Wt	<i>del/del</i>	Wt	<i>del/del</i>	Wt	<i>del/del</i>
12:0	0.03	0.06	0.46	0.97	1.09	1.4
14:0	1.12	0.66	1.88	5.56	n.d.	n.d.
16:0	15.6	9.2	26.7	84.7	1.36	1.26
18:0	11.4	9.12	1.4	2.37	9.24	4.64
18:1	n.d.	n.d.	0.06	n.d.	1.36	1.54
20:0	0.37	0.27	2.91	2.04	26	27
22:0	5.35	1.31	37	n.d.	42.3	53.4
24:0	23.7	39.5	n.d.	n.d.	5.81	4.84
24:1	n.d.	n.d.	n.d.	n.d.	2.56	4.72
26:0	20.3	39.4	1	4.42	0.77	1.27
28:0	1.09	0.39	29.6	n.d.	n.d.	n.d.
30:0	20.8	0.15	n.d.	n.d.	3.18	n.d.
32:0	0.14	n.d.	n.d.	n.d.	6.3	n.d.
34:0	0.1	n.d.	n.d.	n.d.	n.d.	n.d.
Total	100	100	100	100	100	100
Total ^b						
	Wt	<i>del/del</i>				
Total Non-OH	153.4	149.2				
Total α-OH	24.9	5.1				
Total ω-OH	20.2	24.2				
Total	198.5	178.5				

n.d., not detectable.

Polyunsaturated fatty acids were not quantified in epidermis.

^aData are reported as mol % of total FFA.

^bData are reported as nmol/mg of dry epidermis.

whole skin extracts. Analysis of FFA revealed increased total saturated FA (esp. 24:0 and 26:0), while both monounsaturated FA and PUFA (i.e., 18:1n-9, 18:2n-6, and 22:6n-3) were decreased in whole skin from *Elovl4^{del/del}* mouse compared with that from Wt animals (Table 4). A similar trend of increased saturated FA (esp. 16:0, 24:0 and 26:0), and decreased monounsaturated FA (e.g., 18:1n9, 20:1n9) and PUFA (most notably, 18:2) was also evident in the neutral lipid fraction from *Elovl4^{del/del}* mouse skin compared with Wt controls (Table 4). Finally, although the total saturated and unsaturated FA ratios from the polar lipid fraction were largely unchanged, the relative percent of 22:5n3 decreased in *Elovl4^{del/del}* whole skin (Table 4). These results demonstrate that ELOVL4 affects not only VLFA synthesis, but also the generation/distribution of unsaturated FA, consistent with its putative involvement with PUFA metabolism in retina.

DISCUSSION

In these studies, we generated mice with a 5-bp deletion in the *Elovl4* gene as occurs in autosomal dominant Stargardt-like macular degeneration (STGD3) (7). Both the homozygous (*Elovl4^{del/del}*) and heterozygous (*Elovl4^{+del}*) animals develop to term, revealing no embryonic lethality. In addition, no significant difference in animal size or body weight was evident between all three mouse genotypes (*del/del*, *+del*, Wt) immediately after birth. However, the *Elovl4^{del/del}* mice, which express only the mutant ELOVL4 protein, developed skin abnormalities including scaling and xerosis, and died

within a few hours after birth. Conversely, *Elovl4^{+del}* mice revealed no signs of skin or other abnormalities at birth, and demonstrated comparable postnatal growth with Wt animals. Although histopathological studies revealed no significant abnormalities in extracutaneous tissues, competent epidermal permeability barrier structures; i.e., lamellar membranes, did not form in the extracellular domains of *Elovl4^{del/del}* SC. Thus, in addition to the role(s) for ELOVL4 in retina structure and function, the present findings indicate that this ELOVL family protein is important for cutaneous function and required for mammalian survival. In its absence, the ensuing epidermal permeability barrier abnormality results in dehydration, the apparent cause of early neonatal lethality in *Elovl4^{del/del}* mice.

While the presence of VLFA (>C26) of both esterified and free form have been reported in mammalian tissues i.e., epidermis (26), retina (29), brain (30) and testis (31), the responsible enzymes for VLFA synthesis (>28) have not been delineated in any of these tissues. ELOVL4 belongs to a family of FA elongation enzymes (ELO) which are predicted to participate in the synthesis of long-chain FA; e.g., C22:6n-3 (32,33). The significant diminution of both free VLFA and amide-linked VLFA in ceramide/glucosylceramide (i.e., ≥C28) in the epidermis of *Elovl4^{del/del}* neonates, in comparison with littermate controls (Tables 2 and 3), strongly suggests that ELOVL4 is required for *de novo* VLFA (≥C28) synthesis in this tissue. In addition, the present study reveals that ELOVL4 is uniquely involved in the synthesis of such VLFA (C ≥ 28), which has not previously been reported in mammals. Interestingly, since ELOVL4 is also expressed in retina, brain and testis, it might function to generate VLFA in these tissues, as well. However, neither the presence nor the function of such VLFA has yet been explored in these extracutaneous tissues. Finally, since significant decreases in PUFA (including 22:6n-3) were evident in the FFA fraction and non-polar lipid fraction of *Elovl4^{del/del}* skin, ELOVL4 enzymatic activity may also be important for the synthesis of certain PUFA in the skin and other tissues (2).

The present study provides further insights into the mechanisms that lead to barrier dysfunction in *Elovl4^{del/del}* mice. Most importantly, abnormal LB generation and lamellar membrane structures are predominant in the extracellular domains of *Elovl4^{del/del}* SC. These abnormalities provide a likely structural explanation for the diminished epidermal permeability barrier function in animals lacking normal ELOVL4. Yet, multiple metabolic steps are involved in the maintenance of competent barrier function, including high rates of ceramide, glucosylceramide, cholesterol and FFA syntheses, thereby generating the necessary lipid precursors to nascent LB during keratinocyte differentiation. In addition, secretion of LB containing not only lipid precursors, but also hydrolytic enzymes that are required for the extracellular processing of secreted lipid precursors into the non-polar species that form normal lamellar membranes, is also required. Given these multiple steps, what is the likely biochemical mechanism that underlies the attenuation of lamellar membranes, leading to permeability barrier dysfunction in *Elovl4^{del/del}* mice? Since total cholesterol, FFA, ceramide, glucosylceramide and sphingomyelin contents remain normal in *Elovl4^{del/del}* mice, it is likely that high rates of their syntheses are maintained in mice lacking normal ELOVL4.

Table 4. FA profile (% of total FAs) of lipid fractions from whole skin lipids

FFA fraction	Neutral lipid		Polar lipid	
	Wt %	<i>del/del</i>	Wt %	<i>del/del</i>
16:0	7.51 ± 0.16	5.18 ± 0.13	14:0	1.00 ± 0.01
18:0	23.7 ± 0.86	18.8 ± 0.63	15:0	0.15 ± 0.01
20:0 ^a	0.90 ± 0.04	0.73 ± 0.02	16:0	15.7 ± 0.23
22:0	2.87 ± 0.21	2.66 ± 0.09	18:0	4.67 ± 0.10
24:0 ^a	19.6 ± 1.86	26.7 ± 0.93	20:0	0.37 ± 0.01
25:0	3.47 ± 0.34	4.42 ± 0.11	22:0	1.88 ± 0.07
26:0 ^a	16.1 ± 1.10	26.7 ± 0.78	24:0	14.3 ± 0.53
18:1n9 ^a	14.6 ± 0.38	8.10 ± 0.26	25:0	1.50 ± 0.06
18:1n7	1.39 ± 0.05	1.18 ± 0.05	26:0 ^a	3.73 ± 0.16
18:2n6 ^a	6.62 ± 0.16	2.80 ± 0.06	14:1	0.12 ± 0.01
20:4n6	1.92 ± 0.09	1.78 ± 0.11	16:1n7	3.29 ± 0.05
22:6n3 ^a	1.43 ± 0.04	1.09 ± 0.05	18:1n9 ^a	27.9 ± 0.35
			18:1n7	2.15 ± 0.04
			20:1n9	0.85 ± 0.01
			22:1	0.77 ± 0.03
			24:1n9	0.37 ± 0.01
			18:2n6 ^a	13.8 ± 0.19
			18:3n6	0.37 ± 0.01
			20:2n6	0.56 ± 0.01
			20:3n6	0.54 ± 0.01
			20:4n6	1.87 ± 0.03
			22:4n6 ^a	0.41 ± 0.01
			18:3n3 ^a	0.53 ± 0.01
			20:5n3	0.63 ± 0.01
			22:5n3 ^a	0.67 ± 0.01
			22:6n3 ^a	1.76 ± 0.02
			14:0	0.87 ± 0.11
			15:0	0.21 ± 0.01
			16:0	19.6 ± 0.35
			18:0	4.99 ± 0.22
			20:0	0.39 ± 0.01
			22:0	1.80 ± 0.06
			24:0	18.1 ± 0.62
			25:0	2.09 ± 0.06
			26:0	7.78 ± 0.19
			12:1	0.17 ± 0.01
			14:1	0.27 ± 0.01
			16:1	0.64 ± 0.01
			16:1n7	2.56 ± 0.05
			18:1n9	17.9 ± 0.83
			18:1n7	3.26 ± 0.11
			20:1n9	0.42 ± 0.03
			22:1	0.19 ± 0.01
			24:1n9	1.41 ± 0.09
			18:2n6	8.48 ± 0.44
			18:3n6	0.17 ± 0.01
			20:2n6	0.45 ± 0.03
			20:3n6	0.96 ± 0.03
			20:4n6	11.7 ± 0.71
			22:2n6	0.15 ± 0.01
			22:4n6	1.71 ± 0.07
			22:5n6	0.38 ± 0.02
			24:4n6	0.16 ± 0.01
			24:5n6	0.15 ± 0.01
			18:3n3	0.15 ± 0.01
			20:5n3	0.44 ± 0.01
			22:5n3	1.43 ± 0.04
			22:6n3	6.01 ± 0.33
			24:6n3	0.12 ± 0.00

^aThe mean difference is significant at 0.05 level.

In addition to the loss of functional ELOVL4, the epidermal barrier abnormality in *Elovl4*^{del/del} animals could arise either from accumulation of mutant ELOVL4 protein in keratinocytes, or from an as yet unknown gain-of-function in the mutant protein. However, the abnormalities in LB formation, as well as the paucity of extracellular lamellar membrane structures in the *Elovl4*^{del/del} skin, argue strongly that altered lipid content/distribution is the primary cause for the observed deficiency in barrier function.

Elovl4 is expressed from early embryonic stages, indicating that the presence of functional *Elovl4* is critical during development (3). While epidermal permeability structures are formed in the late embryonic stage (i.e., E17–18 in mouse) (40), whether the deficiency of normal ELOVL4 function affects barrier ontogenesis in embryonic stage(s), or whether the terrestrial environment encountered after birth elicits/unmasks the barrier abnormality in *Elovl4*^{del/del} skin, remains unknown. It is also interesting that although *Elovl4* is expressed in the brain at levels similar to its expression in the skin, no significant developmental abnormalities were noted in the brain(s) of homozygous *Elovl4*^{del/del} mice. Although lack of normal ELOVL4 may yet be found to affect brain function, this aspect could not be studied here as the *Elovl4*^{del/del} mice do not survive beyond postnatal day 0.

Moreover, since *Elovl* 1, 4, 5 and 6 are all expressed in the brain, it may be possible that one of these gene products can compensate for the loss of normal brain ELOVL4 in these animals. In the retina, *Elovl4* is expressed at the highest levels among all tissues surveyed, and *Elovl4* levels in the retina were highest compared with the expression of other *Elovl* genes. However, in the retina, *Elovl4* is primarily localized to the photoreceptor layer that is formed during postnatal development in mice. Thus, as the *Elovl4*^{del/del} mice do not survive beyond a few hours after birth, it again was not possible to evaluate the effect(s) of the lack of functional *Elovl4* on the photoreceptor layer development in the retina. Conversely, mice carrying the 5-bp deletion in the heterozygous state survived beyond 20 months, with no apparent skin abnormalities being noted. Similarly, in both STGD3 patients and *Elovl4* heterozygous knock-out mice, no obvious skin abnormalities have been reported (41). This indicates that *Elovl4* haplo-insufficiency does not significantly affect skin development and/or function. The ELOVL4 5-bp deletion was found to be a dominant mutation causing late-onset photoreceptor degeneration both in patients and in the heterozygous knock-in mouse model (1,7). In cultured cells, the mutant 5-bp-deletion protein was found to recruit Wt ELOVL4 into aggregates (6). Given these results, it has

been hypothesized that the late-onset photoreceptor degeneration observed in the ELOVL4 5-bp deletion heterozygous knock-in mice and in STGD3 patients reflects the cumulative effect of the dominant-negative mutation. However, unlike the photoreceptor cells, the outermost layer of the epidermis, the SC, is shed completely about every 2 weeks in humans, possibly limiting accumulation of ELOVL4 aggregates in epidermal keratinocytes of heterozygous individuals. Thus, either this lack of ELOVL4 accumulation or the persistence of ELOVL4 activity in the skin of STGD3 patients and mice carrying the 5-bp deletion mutation in the heterozygous state may explain their lack of skin abnormalities.

Earlier and our current studies also indicate that the expression profiles for specific ELOVL4 proteins are related to tissues expressing these genes, suggesting that each *Elovl* may have a unique role(s) in those tissues. For example, both *Elovl1* and *Elovl3* are involved in the formation of saturated and monounsaturated fatty acyl chains containing up to 24 carbon atoms. *Elovl3*-ablated mice demonstrated dry fur, atrophic sebaceous glands in addition to abnormalities in the regulation of saturated and monounsaturated (n-9) FA levels (42). Although the highest level of *Elovl3* expression is observed in the liver, loss of this gene did not affect the liver function in *Elovl3*-ablated mice. However, the skin, with low baseline levels of *Elovl3* expression, showed a significant defect in water repulsion and increased transepidermal water loss in *Elovl3*-ablated mice (42), suggesting that active ELOVL3 is critical for the normal function of the skin. Together, these results demonstrate important role(s) for long-chain FA in the normal structure and function of the mammalian skin as a barrier to water loss. In addition, these studies reveal the critical role of ELOVL4 in synthesizing the very long-chain FAs and omega-O-acyl ceramides in mammalian tissue and further establish the importance of these unique lipids in mammalian skin structure and function.

MATERIALS AND METHODS

Reagents and antibodies

Anti-ELOVL4 antibody used for immunoblot analysis was from ABCAM (Cambridge, MA, USA). Affinity purified anti-ELOVL4 antibodies used for immunohistochemical analysis were described earlier (43). Anti-filaggrin antibody, anti-loricrin antibody (1:500 dilution), anti-K5 antibody, anti-K1 antibody were from Covance (Berkeley, CA). Alexa fluor-555 and Alexa fluor-448 were from Molecular Probes (Carlsbad, CA); Trizol was from Invitrogen (Carlsbad, CA); Ceramide, glucosylceramide and sphingomyelin were from Matreya (Pleasant Gap, PA) or Avanti Polar Lipids (Alabaster, AL). Cholesterol and palmitic acid were from Sigma-Aldrich (St Louis, MO). Other reagents were purchased from Sigma-Aldrich. High performance thin layer chromatography plates (Silica Gel 60) were from Merck (Darmstadt, Germany).

Animal maintenance and tissue collection

Generation of *Elovl4* 5-bp deletion mutant knock-in mice is described elsewhere (7). Experiments were conducted in accordance with the Statement for the Use of Animals in

Ophthalmic and Vision Research and with protocols approved by the University committee for the use and care of animals. Mice carrying the *Elovl4* 5-bp deletion in the homozygous state were generated by mating heterozygous mice. Neonates were collected immediately after birth to perform the studies described here, and genotypes were monitored by PCR using tail DNA, as described earlier (2). All studies described here were performed on mice carrying the *Elovl4* mutation in the homozygous (*Elovl4^{del/del}*) or heterozygous (*Elovl4^{+del}*) state and with Wt, littermate controls. Adult C57BL/6 mice were used to study the expression profile of different *Elovl4* genes in mouse tissues.

Isolation of RNA and real-time qRT-PCR

Skin from newborn *Elovl4* 5-bp deletion mutant knock-in mice was collected to measure the expression levels of Wt and mutant *Elovl4* alleles. To evaluate the tissue-specific distribution of different *Elovl* genes (i.e., *Elovl1*–*Elovl6*) skin, liver, brain and retina were collected from C57BL/6 mice. Total RNA was isolated using Trizol reagent following manufacturer's instructions.

Isolated RNA was treated with RNase-free DNase I and purified with RNeasy mini kit (Qiagen, Valencia, CA). First strand cDNA was synthesized using random primers and the superscriptTM first strand synthesis system for RT-PCR (Invitrogen). Quantitative PCR and melt curve analysis were performed using BIO-RAD iQTM SYBR Green supermix and a BIO-RAD iCycler (Biorad, Hercules, CA). Relative quantitative expression of genes were calculated by the comparative Ct method, normalized against the housekeeping-gene expression; values are reported as the mean (\pm SD) on an arbitrary scale, as previously reported (3). The list of primers used for the individual *Elovl*s was reported previously (7).

Immunoblot analysis

Protein extracts from skin samples of *Elovl4^{del/del}*, *Elovl4^{+del}* and Wt animals were collected by homogenizing the skin with lysis buffer; protein concentrations were determined using the Pierce BCA reagent (Pierce Biotechnology, Rockford, IL). Proteins were resolved by 10% SDS-PAGE, transferred to nitrocellulose membranes and processed for immunoblot analysis using anti-ELOVL4 antibodies, as previously described (6,43).

Skin histology and ultrastructure

Skin samples from euthanized *Elovl4^{del/del}*, *Elovl4^{+del}* and Wt mice were fixed in formalin and embedded in paraffin. Five-micron sections were cut from each block and stained with hematoxylin and eosin according to standard protocols. For ultrastructural analysis, small pieces of full-thickness skin from neonates were pre-fixed in a mixed aldehyde solution, post-fixed in both osmium tetroxide and ruthenium tetroxide and embedded in an Epon-epoxy resin. Ultrathin sections were examined, after further contrasting with lead citrate, with a Zeiss 1A electron microscope operated at 60 kV.

Hematoxylin staining to assess skin barrier function

To assess epidermal barrier function in animals from each genotype, a skin permeability assay was performed as previously described (44). In brief, newborn animals were euthanized, then fixed in methanol for 5 min, washed with phosphate buffered-saline and incubated in hematoxylin solution for 20 min at room temperature. Excess hematoxylin was removed by several thorough washes with phosphate buffered-saline. After the hematoxylin staining, images of the embryos were captured using a Nikon digital camera.

Immunohistochemistry

Paraffin-embedded skin sections from *Elovl4^{del/del}*, *Elovl4^{+/-del}* and Wt animals were deparaffinized and rehydrated with serial dilutions of alcohol. Immunohistochemistry with anti-filaggrin, anti-loricrin, anti-K5 and anti-K1 antibodies was performed as described previously (7). Fluorescent images were captured by using Nikon-E800 epifluorescence microscope.

Epidermal lipid quantification

Epidermis was separated from dermis as described previously (24). Total epidermal lipids were extracted by the method of Bligh and Dyer (45), as previously modified (24). Briefly, total lipids were extracted from epidermis with chloroform-methanol-water (1:2:0.8) followed by addition of one volume of chloroform and one volume of water to form two layers. Following centrifugation, the lipid-enriched lower phase was mixed with water saturated with chloroform-methanol, and recentrifuged. The lower phase was used for lipid analysis. The major lipid species were separated first by high performance thin-layer chromatography (46,47), with the following solvent systems: (a) for ceramides and glucosylceramides: chloroform-methanol-water (40:10:1, v/v/v) to 2 cm and then to 5 cm; chloroform-methanol-acetic acid (47:2:0.5, v/v/v) to 8.5 cm; and *n*-hexane-diethyl ether-acetic acid (65:35:1, v/v/v) to the top of the plate; (b) for sphingomyelin: chloroform-methanol-acetic acid-water (50:30:8:4, v/v) and (c) for cholesterol and FAs: *n*-hexane-diethyl ether-acetic acid (70:30:1, v/v/v) twice to top of the plate. Lipids were visualized after treatment with cupric acetate-phosphoric acid, and heating to 160°C for 15 min. The quantity of each lipid was determined by spectrodensitometry, as previously described (37). Results are reported as the lipid amount per weight of dry epidermis, and the percent of lipids for particular lipid classes.

Analysis of epidermal amide-linked FA of ceramide/glucosylceramide and FFA by GLC-MS

The ceramide/glucosylceramide fraction was isolated from total epidermal lipid extracts as described previously (46,47). Briefly, total lipid extracts were first applied to an aminopropyl silica gel column (Varian Assoc. Inc., Harbor City, CA), equilibrated with *n*-hexane to separate the ceramide and glucosylceramide containing fraction from the FFA fraction. After washing the column with *n*-hexane, the

fraction containing ceramide/glucosylceramide was eluted with chloroform-isopropanol (2:1, v/v). The FFA fraction was then eluted with 2% acetic acid in diethylether. The ceramide/glucosylceramide containing fraction was subjected to mild alkaline hydrolysis, and then enriched on an aminopropyl silica gel column, as earlier. To quantify the FA composition of ceramide/glucosylceramide, a mixture of odd-chain FA (C15-C25) was added to each sample as internal standards. Following alkaline hydrolysis (4 N KOH, 65°C overnight), FAs from the amide-linked FA of ceramide/glucosylceramide-enriched fraction were converted to their respective methyl esters by incubation with anhydrous methanolic HCl (65°C for 45 min); the resulting FA methylesters were then derivatized to trimethylsilyl ethers, as described previously (48). Derivatives were analyzed by GLC-MS (GCMS-QP2010, Shimadzu Scientific, Columbia, MD) on a Restek RTX-5 column (30 × 0.25 mm I.D., 0.25 μm D.F., Restek Corporation Bellefonte, PA). The initial temperature was 110°C with 10°C increases each minute up to 300°C. Carbon chain length of C12-C34 of saturated FA and unsaturated FA of C18:1 and C24:1, which are present in epidermal ceramides and glucosylceramides, were assessed (46). PUFAs were not quantified in epidermis.

Analysis of epidermal ceramide/glucosylceramide species by APCI tandem mass spectrometry

Sphingolipid species were analyzed using non-aqueous reverse phase HPLC followed by APCI-MS/MS, as described previously (49,50). Briefly, sphingolipids were separated by HPLC on a C18 column using a mobile phase gradient (from methanol with 2% water to methanol with 70% ethyl acetate). The effluent from the HPLC column was continuously ionized by APCI using a Turbo V™ ion source (Applied Biosystems, Framingham, MA). A 3200 Q TRAP® mass spectrometer was operated, while using an information-dependent acquisition (IDA) method, to continuously acquire HPLC-MS data and to automatically collect MS/MS on many of the individual lipids as they eluted. During the IDA runs, molecular weight and abundance information was continuously recorded using a 4000 amu/s EMS, trap MS scan. During each 1 s or shorter acquisition cycle, the most rapidly increasing mass signal detected by the EMS scan was automatically selected as the precursor ion of a trap product ion scan, EPI. The EPI results were then recorded in experiment two using the same time axis. The Analyst® and MarkerView™ software packages used for data analysis associate the HPLC, MS and MS/MS data as a single multidimensional data set. Source conditions, including nebulizer gas flow, nebulizer temperature, nebulizer current, decluster potential, collision energy and collision energy spread had been optimized for both positive and negative ion runs using standard ceramides and cerebrosides.

Analysis of FFA and esterified-FA in whole skin

Full-thickness skin samples (~0.5 cm²) comprising epidermis and dermis and including variable amounts of subcutaneous fat were collected from the dorsal region of newborn mice, weighed and lipid extraction was performed according to the

method of Folch *et al.* (51). Each sample was initially homogenized with 1 ml of BHT-methanol (50 mg/l) and a mixture of internal standards (5.22 µg of 19:1—triglyceride for neutral lipids, 5 µg of 21:0—unesterified FA for the FFA and 6.55 µg of 23:0—phosphatidylcholine for polar lipids/phospholipids) was added.

The lipid fractions, FFA, neutral lipid and polar lipid were obtained by solid phase extraction as previously described (52) and subsequently transmethylated using the BF₃-methanol method of Morrison and Smith (53) as modified by Salem *et al.* (54) with the co-solvent hexane. The methyl ester samples were analyzed by gas chromatography as previously described (54), except that each fraction was injected using a splitless method. For the splitless injection of 1 µl of the hexane extract, the purge flow to the split vent was set to a rate of 14 ml/min and the valve opened 0.25 min after injection.

Statistical analysis

Statistical analysis was performed using the statistical software package SPSS, version 12.0 for Windows (SPSS Inc., Chicago, IL). The results are expressed as mean ± SD for each group. The Kruskal–Wallis test was performed to assess the differences between the means.

ACKNOWLEDGEMENTS

The authors thank Austra Liepa (University of Michigan) for maintaining and generating the animals, Mitchell Gillett (University of Michigan) for histological sectioning, Erby Wilkinson for histopathological evaluation of the pups, Venkat Mocherla for technical assistance at the initial stages of these studies and Debra A. Crumrine for ultrastructural analysis (University of California, San Francisco, CA). This work is supported in part by NIH grants EY13198 (R.A.), AR051077 (Y.U.), AR19098 (P.M.E. and W.M.H.), AR39948 (P.M.E. and W.M.H.), AR045973 (A.D.), Department of Veterans Affairs Merit Review Program (P.M.E. and W.M.H.), NIH core grants to University of Michigan, Department of Ophthalmology and Visual Sciences (EY07003, EY07060), the Foundation Fighting Blindness (R.A.), Research to Prevent Blindness Inc., USA (R.A.) and NIAAA Intramural Research Program (N.S.).

Conflict of Interest statement. None declared.

REFERENCES

- Griesinger, I.B., Sieving, P.A. and Ayyagari, R. (2000) Autosomal dominant macular atrophy at 6q14 excludes *CORD7* and *MCDRL1/PBCRA* loci. *Invest. Ophthalmol. Vis. Sci.*, **41**, 248–255.
- Zhang, K., Kniazeva, M., Han, M., Li, W., Yu, Z., Yang, Z., Li, Y., Metzker, M.L., Allikmets, R., Zack, D.J. *et al.* (2001) A 5-bp deletion in *ELOVL4* is associated with two related forms of autosomal dominant macular dystrophy. *Nat. Genet.*, **27**, 89–93.
- Mandal, M.N., Ambasadhan, R., Wong, P.W., Gage, P.J., Sieving, P.A. and Ayyagari, R. (2004) Characterization of mouse orthologue of *ELOVL4*: genomic organization and spatial and temporal expression. *Genomics*, **83**, 626–635.
- Bernstein, P.S., Tammur, J., Singh, N., Hutchinson, A., Dixon, M., Pappas, C.M., Zabriskie, N.A., Zhang, K., Petrukhin, K., Leppert, M. *et al.* (2001) Diverse macular dystrophy phenotype caused by a novel complex mutation in the *ELOVL4* gene. *Invest. Ophthalmol. Vis. Sci.*, **42**, 3331–3336.
- Maugeri, A., Meire, F., Hoyng, C.B., Vink, C., Van Regemorter, N., Karan, G., Yang, Z., Cremers, F.P. and Zhang, K. (2004) A novel mutation in the *ELOVL4* gene causes autosomal dominant Stargardt-like macular dystrophy. *Invest. Ophthalmol. Vis. Sci.*, **45**, 4263–4267.
- Vasireddy, V., Vijayarathy, C., Huang, J., Wang, X.F., Jablonski, M.M., Petty, H.R., Sieving, P.A. and Ayyagari, R. (2005) Stargardt-like macular dystrophy protein *ELOVL4* exerts a dominant negative effect by recruiting wild-type protein into aggregates. *Mol. Vis.*, **11**, 665–676.
- Vasireddy, V., Jablonski, M.M., Mandal, M.N., Raz-Prag, D., Wang, X.F., Nizol, L., Iannaccone, A., Musch, D.C., Bush, R.A., Salem, N. Jr *et al.* (2006) *Elovl4* 5-bp-deletion knock-in mice develop progressive photoreceptor degeneration. *Invest. Ophthalmol. Vis. Sci.*, **47**, 4558–4568.
- Fuchs, E. and Raghavan, S. (2002) Getting under the skin of epidermal morphogenesis. *Nat. Rev. Genet.*, **3**, 199–209.
- Elias, P.M. and Menon, G.K. (1991) Structural and lipid biochemical correlates of the epidermal permeability barrier. *Adv. Lipid Res.*, **24**, 1–26.
- Schurer, N.Y. and Elias, P.M. (1991) The biochemistry and function of stratum corneum lipids. *Adv. Lipid Res.*, **24**, 27–56.
- Holleran, W.M., Takagi, Y. and Uchida, Y. (2006) Epidermal sphingolipids: metabolism, function, and roles in skin disorders. *FEBS Lett.*, **580**, 5456–5466.
- Man, M.Q., Feingold, K.R. and Elias, P.M. (1993) Exogenous lipids influence permeability barrier recovery in acetone-treated murine skin. *Arch. Dermatol.*, **129**, 728–738.
- Rissmann, R., Groenink, H.W., Weerheim, A.M., Hoath, S.B., Ponec, M. and Bouwstra, J.A. (2006) New insights into ultrastructure, lipid composition and organization of vernix caseosa. *J. Invest. Dermatol.*, **126**, 1823–1833.
- Wertz, P.W., Madison, K.C. and Downing, D.T. (1989) Covalently bound lipids of human stratum corneum. *J. Invest. Dermatol.*, **92**, 109–111.
- Kalinin, A.E., Kajava, A.V. and Steinert, P.M. (2002) Epithelial barrier function: assembly and structural features of the cornified cell envelope. *Bioessays*, **24**, 789–800.
- Hohl, D., Ruf Olano, B., de Viragh, P.A., Huber, M., Detrisac, C.J., Schnyder, U.W. and Roop, D.R. (1993) Expression patterns of lorincrin in various species and tissues. *Differentiation*, **54**, 25–34.
- Roop, D. (1995) Defects in the barrier. *Science*, **267**, 474–475.
- Fuchs, E. (1995) Keratins and the skin. *Annu. Rev. Cell. Dev. Biol.*, **11**, 123–153.
- Williams, M.L. (1991) Lipids in normal and pathological desquamation. *Adv. Lipid Res.*, **24**, 211–262.
- Hardman, M.J., Sisi, P., Banbury, D.N. and Byrne, C. (1998) Patterned acquisition of skin barrier function during development. *Development*, **125**, 1541–1552.
- Hou, S.Y., Mitra, A.K., White, S.H., Menon, G.K., Ghadially, R. and Elias, P.M. (1991) Membrane structures in normal and essential fatty acid-deficient stratum corneum: characterization by ruthenium tetroxide staining and x-ray diffraction. *J. Invest. Dermatol.*, **96**, 215–223.
- Elias, P.M., Schmuth, M., Uchida, Y., Rice, R.H., Behne, M., Crumrine, D., Feingold, K.R., Holleran, W.M. and Pharm, D. (2002) Basis for the permeability barrier abnormality in lamellar ichthyosis. *Exp. Dermatol.*, **11**, 248–256.
- Ladd, P.A., Du, L., Capdevila, J.H., Mernaugh, R. and Keeney, D.S. (2003) Epoxyeicosatrienoic acids activate transglutaminases *in situ* and induce cornification of epidermal keratinocytes. *J. Biol. Chem.*, **278**, 35184–35192.
- Uchida, Y., Hara, M., Nishio, H., Sidransky, E., Inoue, S., Otsuka, F., Suzuki, A., Elias, P.M., Holleran, W.M. and Hamanaka, S. (2000) Epidermal sphingomyelins are precursors for selected stratum corneum ceramides. *J. Lipid Res.*, **41**, 2071–2082.
- Ponec, M., Weerheim, A., Lankhorst, P. and Wertz, P. (2003) New acylceramide in native and reconstructed epidermis. *J. Invest. Dermatol.*, **120**, 581–588.
- Stewart, M.E. and Downing, D.T. (1999) A new 6-hydroxy-4-sphingenine-containing ceramide in human skin. *J. Lipid Res.*, **40**, 1434–1439.

27. Bouwstra, J.A., Gooris, G.S., Dubbelaar, F.E. and Ponc, M. (2001) Phase behavior of lipid mixtures based on human ceramides: coexistence of crystalline and liquid phases. *J. Lipid. Res.*, **42**, 1759–1770.
28. Paige, D.G., Morse-Fisher, N. and Harper, J.I. (1994) Quantification of stratum corneum ceramides and lipid envelope ceramides in the hereditary ichthyoses. *Br. J. Dermatol.*, **131**, 23–27.
29. Rotstein, N.P. and Avelandano, M.I. (1988) Synthesis of very long chain (up to 36 carbon) tetra, penta and hexaenoic fatty acids in retina. *Biochem. J.*, **249**, 191–200.
30. Martinez, M. and Mougan, I. (1998) Fatty acid composition of human brain phospholipids during normal development. *J. Neurochem.*, **71**, 2528–2533.
31. Robinson, B.S., Johnson, D.W. and Poulos, A. (1992) Novel molecular species of sphingomyelin containing 2-hydroxylated polyenoic very-long-chain fatty acids in mammalian testes and spermatozoa. *J. Biol. Chem.*, **267**, 1746–1751.
32. Cinti, D.L., Cook, L., Nagi, M.N. and Suneja, S.K. (1992) The fatty acid chain elongation system of mammalian endoplasmic reticulum. *Prog. Lipid. Res.*, **31**, 1–51.
33. Tvrdik, P., Westerberg, R., Silve, S., Asadi, A., Jakobsson, A., Cannon, B., Loison, G. and Jacobsson, A. (2000) Role of a new mammalian gene family in the biosynthesis of very long chain fatty acids and sphingolipids. *J. Cell. Biol.*, **149**, 707–718.
34. Holleran, W.M., Ginns, E.L., Menon, G.K., Grundmann, J.U., Fartasch, M., McKinney, C.E., Elias, P.M. and Sidransky, E. (1994) Consequences of beta-glucocerebrosidase deficiency in epidermis. Ultrastructure and permeability barrier alterations in Gaucher disease. *J. Clin. Invest.*, **93**, 1756–1764.
35. Doering, T., Holleran, W.M., Potratz, A., Vielhaber, G., Elias, P.M., Suzuki, K. and Sandhoff, K. (1999) Sphingolipid activator proteins are required for epidermal permeability barrier formation. *J. Biol. Chem.*, **274**, 11038–11045.
36. Bouwstra, J.A., Gooris, G.S., Dubbelaar, F.E., Weerheim, A.M., Ijzerman, A.P. and Ponc, M. (1998) Role of ceramide 1 in the molecular organization of the stratum corneum lipids. *J. Lipid. Res.*, **39**, 186–196.
37. Behne, M., Uchida, Y., Seki, T., de Montellano, P.O., Elias, P.M. and Holleran, W.M. (2000) Omega-hydroxyceramides are required for corneocyte lipid envelope (CLE) formation and normal epidermal permeability barrier function. *J. Invest. Dermatol.*, **114**, 185–192.
38. Melton, J.L., Wertz, P.W., Swartzendruber, D.C. and Downing, D.T. (1987) Effects of essential fatty acid deficiency on epidermal O-acylsphingolipids and transepidermal water loss in young pigs. *Biochim. Biophys. Acta.*, **921**, 191–197.
39. Imokawa, G., Abe, A., Jin, K., Higaki, Y., Kawashima, M. and Hidano, A. (1991) Decreased level of ceramides in stratum corneum of atopic dermatitis: an etiologic factor in atopic dry skin? *J. Invest. Dermatol.*, **96**, 523–526.
40. Hanley, K., Devaskar, U.P., Hicks, S.J., Jiang, Y., Crumrine, D., Elias, P.M., Williams, M.L. and Feingold, K.R. (1997) Hypothyroidism delays fetal stratum corneum development in mice. *Pediatr. Res.*, **42**, 610–614.
41. Raz-Prag, D., Ayyagari, R., Fariss, R.N., Mandal, M.N., Vasireddy, V., Majchrzak, S., Webber, A.L., Bush, R.A., Salem, N. Jr, Petrukhin, K. *et al.* (2006) Haploinsufficiency is not the key mechanism of pathogenesis in a heterozygous elovl4 knockout mouse model of STGD3 disease. *Invest. Ophthalmol. Vis. Sci.*, **47**, 3603–3611.
42. Westerberg, R., Tvrdik, P., Unden, A.B., Mansson, J.E., Norlen, L., Jakobsson, A., Holleran, W.H., Elias, P.M., Asadi, A., Flodby, P. *et al.* (2004) Role for ELOVL3 and fatty acid chain length in development of hair and skin function. *J. Biol. Chem.*, **279**, 5621–5629.
43. Ambasadhan, R., Wang, X., Jablonski, M.M., Thompson, D.A., Lagali, P.S., Wong, P.W., Sieving, P.A. and Ayyagari, R. (2004) Atrophic macular degeneration mutations in ELOVL4 result in the intracellular misrouting of the protein. *Genomics*, **83**, 615–625.
44. Stone, S.J., Myers, H.M., Watkins, S.M., Brown, B.E., Feingold, K.R., Elias, P.M. and Farese, R.V. Jr. (2004) Lipopenia and skin barrier abnormalities in DGAT2-deficient mice. *J. Biol. Chem.*, **279**, 11767–11776.
45. Bligh, E.G. and Dyer, W.J. (1959) A rapid method of total lipid extraction and purification. *Can. J. Biochem. Physiol.*, **37**, 911–917.
46. Hamanaka, S., Hara, M., Nishio, H., Otsuka, F., Suzuki, A. and Uchida, Y. (2002) Human epidermal glucosylceramides are major precursors of stratum corneum ceramides. *J. Invest. Dermatol.*, **119**, 416–423.
47. Uchida, Y., Behne, M., Quiec, D., Elias, P.M. and Holleran, W.M. (2001) Vitamin C stimulates sphingolipid production and markers of barrier formation in submerged human keratinocyte cultures. *J. Invest. Dermatol.*, **117**, 1307–1313.
48. Alderson, N.L., Walla, M.D. and Hama, H. (2005) A novel method for the measurement of *in vitro* fatty acid 2-hydroxylase activity by gas chromatography-mass spectrometry. *J. Lipid. Res.*, **46**, 1569–1575.
49. Munoz-Garcia, A., Ro, J., Brown, J.C. and Williams, J.B. (2006) Identification of complex mixtures of sphingolipids in the stratum corneum by reversed-phase high-performance liquid chromatography and atmospheric pressure photospray ionization mass spectrometry. *J. Chromatogr. A*, **1133**, 58–68.
50. Henion, J.D., Thomson, B.A. and Dawson, P.H. (1982) Determination of sulfa drugs in biological fluids by liquid chromatography/mass spectrometry/mass spectrometry. *Anal. Chem.*, **54**, 451–456.
51. Folch, J., Lees, M. and Sloane Stanley, G.H. (1957) A simple method for the isolation and purification of total lipides from animal tissues. *J. Biol. Chem.*, **226**, 497–509.
52. Kim, H.Y. and Salem, N. Jr. (1990) Separation of lipid classes by solid phase extraction. *J. Lipid. Res.*, **31**, 2285–2289.
53. Morrison, W.R. and Smith, L.M. (1964) Preparation of fatty acid methyl esters and dimethylacetals from lipids with boron fluoride-methanol. *J. Lipid. Res.*, **5**, 600–608.
54. Salem, N. Jr, Reyzer, M. and Karanian, J. (1996) Losses of arachidonic acid in rat liver after alcohol inhalation. *Lipids*, **31** (suppl), S153–S156.